HHS Public Access

Author manuscript

Acta Biomater. Author manuscript; available in PMC 2019 July 15.

Published in final edited form as:

Acta Biomater. 2018 July 15; 75: 427–438. doi:10.1016/j.actbio.2018.05.051.

Nanopatterned Bulk Metallic Glass-based Biomaterials Modulate Macrophage Polarization

Mahdis Shayan[a], **Jagannath Padmanabhan**[b], **Aaron H. Morris**[b], **Bettina Cheung**[b], **Ryan Smith**[b], **Jan Schroers**[b,c], and **Themis R. Kyriakides**[a,b,*]

[a]Department of Pathology, Yale University, New Haven, CT 06520, USA

[b]Department of Biomedical Engineering, Yale University, New Haven, CT 06520, USA

[c]Department of Mechanical Engineering and Materials Science, Yale University, New Haven, CT 06520, USA

Abstract

Polarization of macrophages by chemical, topographical and mechanical cues presents a robust strategy for designing immunomodulatory biomaterials. Here, we studied the ability of nanopatterned bulk metallic glasses (BMGs), a new class of metallic biomaterials, to modulate murine macrophage polarization. Cytokine/chemokine analysis of IL-4 or IFNγ/LPS-stimulated macrophages showed that the secretion of TNF-α, IL-1α, IL-12, CCL-2 and CXCL1 was significantly reduced after 24-hour culture on BMGs with 55nm nanorod arrays (BMG-55). Additionally, under these conditions, macrophages increased phagocytic potential and exhibited decreased cell area with multiple actin protrusions. These *in vitro* findings suggest that nanopatterning can modulate biochemical cues such as IFNγ/LPS. *In vivo* evaluation of the subcutaneous host response at 2 weeks demonstrated that the ratio of Arg-1 to iNOS increased in macrophages adjacent to BMG-55 implants, suggesting modulation of polarization. In addition, macrophage fusion and fibrous capsule thickness decreased and the number and size of blood vessels increased, which is consistent with changes in macrophage responses. Our study demonstrates that nanopatterning of BMG implants is a promising technique to selectively polarize macrophages to modulate the immune response, and also presents an effective tool to study mechanisms of macrophage polarization and function.

Graphical Abstract

Implanted biomaterials elicit a complex series of tissue and cellular responses, termed the foreign body response (FBR), that can be influenced by the polarization state of macrophages. Surface topography can influence polarization, which is broadly characterized as either inflammatory or repair-like. The latter has been linked to improved outcomes of the FBR. However, the impact of topography on macrophage polarization is not fully understood, in part, due to a lack of high moduli biomaterials that can be reproducibly processed at the nanoscale. Here, we studied

*Corresponding author: Phone: +1-203-737-2214. themis.kyriakides@yale.edu.

macrophage interactions with nanopatterned bulk metallic glasses (BMGs), a class of metallic alloys with amorphous microstructure and formability like polymers. We show that nanopatterned BMGs modulate macrophage polarization and transiently induce less fibrotic and more angiogenic responses. Overall, we demonstrate nanopatterning of BMG implants as a technique to polarize macrophages and modulate the FBR.

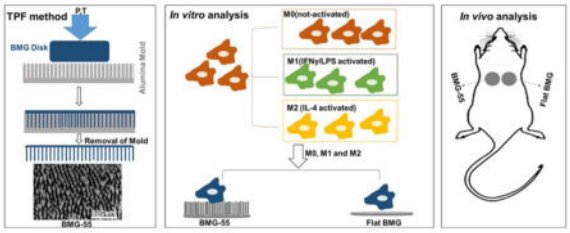

Keywords

Bulk metallic glass; Macrophage polarization; Nanopatterning; Foreign body response; Cytokines

1. Introduction

Implantation of medical devices and biomaterials results in tissue injury and triggers the inflammation process, which is extended in the presence of a biomaterial [1–3]. Typically, the host tissue response to implants leads to a unique sequence of molecular and cellular events known as the foreign body response (FBR) that results in the encapsulation of biomaterials by a mostly avascular collagenous capsule. Because of this response, there is suboptimal biomaterial integration within tissue, which can lead to compromised function and subsequent failure. Thus, to improve the quality of implants and prolong their lifetime, it is essential to develop strategies to mitigate the FBR.

Macrophages are phagocytic leukocytes, which are recruited following implantation and adhere to the biomaterial surface. They play a pivotal role in orchestrating the host response either directly or through modulating the function of other cell types such as lymphocytes, endothelial cells, and fibroblasts [4, 5]. In addition, macrophages can undergo fusion to form multinucleated foreign body giant cells (FBGC), which is a hallmark of the FBR [6, 7]. Moreover, macrophages release a wide spectrum of chemokines and cytokines as well as growth factors that orchestrate tissue remodeling processes. These include the recruitment and activation of inflammatory cells, resolution of inflammation, debris scavenging, and angiogenesis [4, 6, 8]. The nature and level of the released biomolecules depend on the phenotype of macrophages, which are characterized based on their cytokine and gene expression profiles, cell surface molecules, and cell morphology [9–12]. Detailed descriptions of different macrophage phenotypes have been recently provided in extensive reviews [13–15]; for example, classically activated pro-inflammatory macrophages or M1 macrophages are induced by interferon-gamma (IFN-γ)/lipopolysaccharide (LPS). Following stimulation, inducible nitric oxide synthase (iNOS) is expressed leading to subsequent nitric oxide (NO) production that upregulates the production of a variety of inflammatory cytokines and mediators such as interleukin (IL)-1β and tumor necrosis factor

(TNF). In contrast, macrophages activated by IL-4 are known as alternatively activated macrophages or M2 macrophages; they show anti-inflammatory properties by suppressing the production of inflammatory cytokines and by expressing arginase-1(Arg-1) instead of iNOS [16, 17].

Several studies have reported the plasticity and rapid shift in macrophage phenotypes in response to local environmental factors presented as chemical, mechanical, and/or topographical cues [18–24]. For example, functionalization of the surface of poly (ethylene glycol)-based hydrogels with arginine-glycine-aspartate (RGD) peptide, has been shown to significantly reduce the expression of the pro-inflammatory cytokines TNF-α and IL-1β in bone-marrow derived murine macrophages (BMDMs) and mitigate the FBR [25]. In another study, macrophages on poly (ethylene glycol)-RGD-based hydrogels with low stiffness (130kPa), expressed less pro-inflammatory cytokines such as TNF-α, IL-1β, and IL-6 when compared to cells on similar substrates with higher compressive moduli (240 and 840kPa) [26]. Such strategies suggest the possible beneficial outcomes of regulating macrophage polarization in order to attenuate biomaterial-induced adverse effects [24–30].

Our group recently demonstrated that nanopatterning the surfaces of platinum-based bulk metallic glasses ($Pt_{57.5}Cu_{14.7}Ni_{5.3}P_{22.5}$, Pt-BMGs) could alter cell behaviors [31, 32]. These studies were made possible because BMGs are amorphous metallic alloys that exhibit unique processing opportunities due to the lack of crystalline order and grains in their atomic microstructure. They also have similar mechanical strength and stiffness to metallic alloys but are highly processable and flexible like polymers, which facilitates manufacturing of precise nanopatterned surfaces through thermoplastic forming (TPF) that cannot be achieved with conventional metals [32–35]. Such nanopatterns induced changes in the cytoskeletal arrangement of various cell types including macrophages [32]. Specifically, we examined the effect of nanopatterning on macrophage morphology and demonstrated changes on arrays of 200nm diameter nanorods (BMG-200) [32]. In a subsequent study, we showed that arrays of 55nm diameter nanorods (BMG-55) could reduce macrophage fusion on BMG substrates *in vitro* and *in vivo* in the short term (7 days) [31], but we did not examine effects on the FBR in the long term. Here, we expanded on these studies by investigating the ability of BMG-55 to modulate the polarization of macrophages in response to IFNγ/LPS or IL-4 *in vitro* and to modulate the FBR *in vivo* at 2 and 4 weeks following implantation. We show that BMG-55 can modulate macrophage polarization and functions *in vitro*. In addition, BMG-55 altered the kinetics of the FBR, characterized by reduced FBGC formation and encapsulation and increased angiogenesis at 2 weeks. These changes were associated with significant shifts in macrophage polarization suggesting that nanopatterning of BMGs can be used as a tool to modulate parameters of the FBR.

2. Materials and methods

2.1. Preparation of BMG samples

Nanopatterned Pt-based BMG ($Pt_{57.5}Cu_{14.7}Ni_{5.3}P_{22.5}$) samples were prepared through thermoplastic deformation as described previously [32, 34, 36]. Briefly, raw materials, including platinum, phosphorus, nickel, and copper were melted and cast in rods of 2mm diameter and 12 mm in length and subsequently fluxed with B_2O_3 and quenched with water.

BMG rods were then cut in 2mm height and 2mm diameter disks and pressed on nanoporous alumina (Al_2O_3) (anodic aluminum oxide (AAO)) of 55nm-diameter pore size at 540K temperature using a molding force of 10kN applied by compression tester (Instron Model 5569). Subsequently, the alumina molds, were removed from the nanopatterned surfaces by etching with a 30% KOH solution.

2.2. *In vitro* studies of macrophage behavior on BMG substrates

2.2.1. Monocyte isolation and macrophage polarization—Bone marrow-derived macrophages (BMDMs) were isolated from 9 to 12 week-old C57BL6 mice as described previously [37]. All procedures were performed in accordance with the protocol approved by the National Institutes of Health (NIH) and the Institutional Animal Care and Use Committee (IACUC) at Yale University. Briefly, mice femurs were harvested for isolating bone marrow cells by flushing the bone shafts using a wash comprising of IMDM media containing 20% FBS and 1% Penicillin-Streptomycin (P/S). Ack-Lysis buffer was used to lyse the red blood cells. Subsequently, the cells were seeded for 4hrs to allow the bone-resident monocytes to adhere, followed by resuspension of the supernatant in media containing 20ng/mL M-CSF. BMDMs were maintained in culture for 7 days and on the fourth day, 10mL media with 20ng/mL M-CSF was added on top of cultured cells. On day 7, the cells were again treated with 10ng/mL M-CSF to be used for the experiment on the following day.

Flat and nanopatterned BMG samples were decontaminated in 70% ethanol for 30min and were subsequently washed with sterilized phosphate buffer saline (PBS) for 5min. Then, each sample was cultured with 5×10^5 cells in 1mL media containing 10ng/mL M-CSF and 100ng/mL FLT-3 ligand. After overnight incubation, the media was aspirated followed by a PBS wash and a replacement with fresh growth medium (DMEM/F12 (1:1) supplemented with 1% P/S, 1% L-glutamine and 10% FBS). To generate classically activated macrophages, cells were seeded with growth media containing 20ng/mL IFN-γ for 6hrs and following PBS rinses, growth media containing 100ng/mL LPS was added for 18hrs. To generate alternatively activated macrophages, cells were cultured with growth media containing 20ng/mL IL-4 for 24hrs.

2.2.2. Luminex-based cytokine detection and quantification—Cultured macrophage supernatants with and without (IFN-γ/LPS) or IL-4 stimulations, were collected and the levels of 23 different chemokines and cytokines were assayed using a Milliplex MAP mouse cytokine/chemokine premixed 23-plex kit (Millipore, Billerica) on a Bio-Plex Suspension Array System (Bio-Rad Laboratories). Cytokines included in the analysis were IL-1α, IL-1β, IL-2, IL-3, IL-4, IL-5, IL-6, IL-9, IL-10, IL-12, IL-13, IL-17, CCL11, G-CSF, GM-CSF, IFN-γ, CXCL1, CCL2, CCL3, CCL4, CCL5, and TNF-α with a typical detection range of 5–100,000pg/ml for each analyte. A total of three independent samples (supernatants) per condition were used for the measurement.

2.2.3. Quantification of macrophage morphology—To assess the morphology of cultured macrophages on BMG substrates, cells were fixed with 4% paraformaldehyde for 20min, washed with PBS and permeabilized with 0.1% Triton X-100 for 5min, then stained

with Rhodamine-Phalloidin for 30min at ambient temperature and counterstained with DAPI. Subsequently, stained cells were imaged using a fluorescent microscope (Zeiss, HBO 100). Five samples per condition were analyzed and shape parameters (area, perimeter and circularity) of 300 individual cells per condition were quantified using NIH Image J software [32]. Average cell area and perimeter indicate cell growth and spreading. Circularity index, which is defined as $[4\pi \times (\text{cell area})/(\text{cell perimeter})^2]$, gets a value between 0(highly elongated polygon) to 1(perfect circle). In addition, morphology of adhered cells was evaluated using SEM after sputtering a thin layer of Iridium (Ir). For SEM imaging, cells were fixed with 2.5% glutaraldehyde, dehydrated in a series of ethanol/DI water mixtures including 30%, 50%, 75%, 90%, and 100% ratios, followed by drying in Hexamethyldisilazane (HMDS) overnight at room temperature.

2.2.4. BMDMs phagocytosis on BMGs—The effect of nanopatterning of BMGs on phagocytosis of cultured macrophages were evaluated *in vitro*. Phagocytosis was induced by adding Fluoresbrite® YG microspheres (Polysciences Inc., Warrington, PA) with 3μm diameter, following the stimulation with IL-4 or IFN-γ/LPS. The spheres were added at 1:5 (cell:sphere) ratio, which is enough to engage most cells in phagocytosis [6, 38]. Following 24hrs incubation with microspheres, cells were washed with PBS, fixed and stained with Rhodamine Phalloidin. Uptake of microspheres was evaluated using fluorescence microscopy and the percentage of cells with spheres and the average number of spheres per cell was measured using Image J software. Five independent samples per condition were analyzed and ten random fluorescent images in each sample were captured for quantification.

2.3. *In vivo* implantation and analysis

Subcutaneous implantations were performed as described previously [38]. A total of six C57BL/6 mice aged 9–12 weeks per time point were used and each mouse received two bilateral implants following midline incision; a flat BMG and a BMG-55 with the nanopatterned side facing the dermis. Equal numbers of male and female mice were used for *in vivo* studies. Animals were sacrificed at 2 and 4 weeks after implantation, and excised implants were removed from their tissue capsule and surrounding tissues. Remaining tissues were fixed in 4% formaldehyde, processed and embedded in paraffin wax for histological analysis. Implants were fixed and prepared for SEM as described above. Tissues were sectioned and stained with Masson's trichrome and five sections per condition were analyzed. Stained sections were visualized using light microscopy (Zeiss, AX10) and fibrous capsule thickness around the implants was measured using MetaMorph software at five random locations.

In addition, immunofluorescence was performed on paraffin-embedded sections. Briefly, for each condition, slides were deparaffinized, rehydrated, blocked and incubated with primary antibodies of rat anti-mouse macrophage antigen-3 (Mac-3) (BD Pharmingen™) along with either a goat polyclonal antibody to arginase-1 (Arg-1) (Santa Cruz Biotechnology, sc-18351) or a rabbit polyclonal antibody to iNOS (abcam, ab15323) overnight at 4°C. The primary antibodies were diluted in 1% BSA/PBS with ratios of 1:10 for Mac-3, 1:50 for Arg-1 and 1:100 for iNOS. After washing, the samples were incubated for 1hr with donkey

anti-rat (Alexa Fluor® 594, ab150156) and donkey anti-goat (Alexa Fluor® 488, ab150129) secondary antibodies for Mac-3/Arg-1 stained sections or donkey anti-rat and goat anti-rabbit (Alexa Fluor® 488, ab150077) secondary antibodies for Mac-3/iNOS stained sections at room temperature. All secondary antibodies were diluted with 1:200 ratio in PBS. Following PBS rinses, the sections were mounted for fluorescence microscopy. Immunofluorescence staining was also performed for the endothelial cell marker, CD31, using a similar approach. Rat monoclonal anti-mouse CD31 (dianova, DIA-310) and donkey anti-rat IgG were used as primary antibody and secondary antibody, respectively. A total of five sections per condition were analyzed. Ten random fluorescent images in each section were captured and the percentage of Arg-1-positive Mac-3 and the percentage of iNOS-positive Mac-3 were measured using Image J software. The number and surface area of vessels (CD31 stained blood vessels) in each captured fluorescent image was measured using Image J software.

Implants, detached from adjacent tissues, were inspected for attached cells and FBGCs using SEM imaging. Three independent samples per condition were prepared following the aforementioned steps; five random fields were imaged in each sample and representative images per condition were presented in the results section.

2.4. Statistical analysis

Results in each experiment were expressed as means + standard deviation (SD). In *in vitro* tests (cytokine/chemokine profiles, macrophage morphology parameters, macrophage phagocytosis), the means response of flat BMG and BMG-55 were compared in each condition using one-way ANOVA test and the criterion of statistical significance was considered P-value ≤ 0.05. In *in vivo* immunofluorescent assays and fibrous capsule thickness measurement, the significance differences between the means response of flat BMG and BMG-55 following 2-week and 4-week implantation were evaluated using one-way ANOVA test with P-value ≤ 0.05. For *in vivo* immunofluorescence experiments, the Tukey post-hoc multiple-comparison analysis was performed as well. Statistical analysis was performed using Minitab® 18 software (Minitab Inc. State College, PA).

3. Results

3.1. Multiplex cytokine/chemokine profiles

To study the polarization of macrophages on flat BMG and BMG-55 substrates, the level of 23 different chemokines and cytokines released by the unstimulated (M0), IFNγ/LPS-stimulated (M1), or IL-4 -stimulated (M2) cells were measured. In each group of cells, the response of flat and nanopatterned substrates was compared to each other. IFNγ/LPS stimulation increases the secretion level of the pro-inflammatory cytokines in M1 cells cultured on flat or nanopatterned BMGs. However, culturing M1 macrophages on BMG-55 substrate significantly reduced the secretion of IL-1α, TNF-α, IL-6, IL-12 (p70) and IL-12 (p40) compared to flat BMG substrate (Fig. 1A).

Similar to pro-inflammatory cytokine profiles, the secretion of the pro-inflammatory chemokines (CCL2, CCL3, CCL4, CCL5, CCL11 and CXC11) increased in classically

activated macrophages. The results demonstrated that nanopatterning can change chemokine secretion such that the level of CCL2, CCL4 and CXCL1 decreased on BMG-55 compared to flat BMG (Fig. 1B). BMG-55 either significantly reduced or caused no significant change on the pro-inflammatory cytokines and chemokines.

IFNγ/LPS and IL-4 stimulations increased the release of IL-4, IL-10 and IL-13; these changes were not affected by nanopatterning (Fig. 2). In M2 macrophages, levels of IL-4 include exogenously added and released; therefore, its levels between groups cannot be directly compared. Release profiles for other cytokines and chemokines can be found in the supplementary materials (Supplementary Figure).

3.2. *In vitro* BMDMs morphology on BMGs

To investigate the association between macrophage shape change and nanopatterning of BMG substrates, we studied actin cytoskeleton arrangement by Phalloidin stain (Fig. 3A) and quantification of shape parameters (area, perimeter and circularity) (Fig. 3B).

IFNγ/LPS stimulation causes cytoskeletal actin re-arrangement on both flat and nanopatterned BMGs. M1 cells on both surfaces became larger and more spread; however, the size of M0 and M1 cells (indicated by average cell perimeter and area) on the flat BMG were significantly larger compared to BMG-55 substrate (Fig. 3Ba–b). In addition to size, cells on BMG-55 showed multiple fine projections on their surfaces, all indicating the influence of nanopatterning on the morphology of macrophages. IL-4 stimulation generally increased elongation of cells on both flat and nanopatterned BMG substrates, while small podia appeared on the surface of cells on BMG-55. The morphology of attached cells was also evaluated using SEM imaging (Fig. 4). Representative SEM images could present the effect of nanopatterning on the morphology of macrophages more clearly and also confirmed the observations of the fluorescent imaging of cytoskeletal actin such as higher spreading of M0 cells on the flat surface (Fig. 4B-a and -d). M1 cells on BMG-55 substrate distinctly demonstrated the podia appearance compared to flat surface (Fig. 4B-b and -e).

3.3. *In vitro* BMDMs phagocytosis on BMGs

Phagocytosis is one of the essential functions of macrophages and we studied whether nanopatterning would influence this process. The uptake of fluorescent microspheres (yellow) by macrophages attached on BMGs was visualized by microscopy (Fig. 5A) and the percentage of cells containing microspheres and number of microspheres per cell were measured (Fig. 5B). Results showed that phagocytosis was enhanced on BMG-55 substrate, indicating that nanopatterning of BMGs can significantly change the phagocytic response in IFN-γ/LPS-treated macrophages. In addition, this finding suggests specificity in the ability of BMG-55 to reduce macrophage fusion as other functions are not compromised.

3.4. BMG implants capsule thickness

Given that significant reduction of pro-inflammatory cytokines release and morphological change of M1 macrophages on BMG-55 during *in vitro* experiments, flat BMG and BMG-55 disks were subcutaneously implanted in WT mice for 2 and 4 weeks to investigate the *in vivo* response. Masson's trichrome-stained sections were used to measure fibrous

capsule thickness around flat BMG and BMG-55 implants in wild type (WT) mice (Fig. 6A–D). Figure 6E and 6F plot average capsule thickness for both implants at 2 and 4-week time points. Capsule thickness values for flat BMG implant sites were found to be 317 ± 22μm and 172 ± 13μm for 2 and 4-week time points, respectively, whereas they were 187 ± 24μm and 201 ± 15μm for BMG-55 implant sites for the same time points. BMG-55 demonstrated significantly thinner capsules after 2 weeks of implantation, suggesting a shift in the kinetics of the FBR.

3.5. *In vivo* evaluation of FBGC formation

To evaluate the formation of macrophage fusion on flat BMG and BMG-55 implants, the surface of explanted BMGs following 2- and 4-week implantation was examined using SEM imaging (Fig. 7). After 2 weeks of implantation, FBGCs are visible on the surface of flat BMG (Fig. 7A), but there was a remarkable attenuation of FBGC formation on BMG-55 (Fig. 7C). Following 4-week implantation, the surface of flat BMG implants was covered with multinuclear giant cells (Fig. 7B); however, the level and size of macrophage fusion on the surface of BMG-55 implants was reduced (Fig. 7D).

3.6. *In vivo* Arg-1 and iNOS expression

The phenotype of the recruited macrophages was determined by double-staining of explanted tissues surrounding the implants for Mac-3/Arg-1 (Fig. 8A) and Mac-3/iNOS (Fig. 8B). Macrophages are identified with Mac-3 positive cells; Arg-1 positive cells indicate M2 cells, while iNOS positive cells indicate M1 cells. The percentage of Arg-1 expression around BMG-55 after 2 weeks significantly increased compared to flat BMG while after 4 weeks, no difference in Arg-1 expression was observed. These results show the ratio of Arg-1 to iNOS expression in macrophages of tissues surrounding BMG-55 implants after 2 weeks significantly increased (Fig. 8C).

3.7. *In vivo* vascularization

In vivo vascularization in tissues surrounding flat BMG and BMG-55 implants was evaluated by quantification of CD31-stained vessels (Fig. 9). Normalized average area of blood vessels, which indicate both the number and size of vessels, increased in tissues surrounding BMG-55 implants following 2-week implantation (Fig. 9I). After 4 weeks, vascularization decreased in tissues around BMG-55. These results indicate the capability of BMG-55 to modulate vascularization of the FBR.

4. Discussion

Results presented in this study demonstrate that nanopatterning of BMG substrates modulates the activation of IFN-γ/LPS treated macrophages, which leads to significant reductions in the secretion of TNF-α and CCL-2 and changes in cell size and shape as well as phagocytosis. Furthermore, BMG-55 implants induced changes in the FBR that were associated with a shift in macrophage polarization.

Macrophage polarization can be modulated to attenuate the FBR by manipulating implant surface characteristics such as roughness, topography, chemistry or surface energy [39–43].

For instance, it was observed that macrophage adhesion and expression of pro-inflammatory markers like TNF-α and CD68 decreased on nanofeatured titanium surfaces [44, 45]. Nano-featured metallic surfaces can be created by multiple techniques like electrochemical anodization, hydrothermal treatment, acid etching and sand blasting [46–50]. However, these methods not only involve long multi-step processes, but also require severe thermal and chemical reactions that result in a non-uniform and random topographies. In contrast, bulk metallic glasses can be used to create a wide range of precisely controlled micro- and nanopatterns with intact surface chemistry [32–35].

Surface nanopatterning alters surface energy such that the wettability of BMG-55 was enhanced relative to flat BMG. These changes can influence the type, level and topography of adsorbed proteins, which subsequently affect interactions with cell surface receptors. For example, in a previous study, we showed that changes in BMG nanopattern dimensions modulated the extent and distribution of fibronectin adsorption [32].

Following implantation and protein adsorption, macrophages adhere on the surface, fuse together and form FBGCs. Cell to cell fusion is a dynamic cellular event that is involved in various physiological processes such as stem cell differentiation and bone remodeling [51–54]. Our previous *in vitro* studies showed that macrophage fusion and FBGC formation was attenuated on nanopatterned BMGs. Specifically, BMG-55 restricted macrophages cytoskeletal remodeling and spreading leading to a change in the activation of p38 MAP kinase that regulates cytoskeleton rearrangement during fusion. Additionally, BMG-55s reduced the formation of FBGCs when implanted in the peritoneum (IP) in WT mice for 1 week [31]. Our present *in viv*o results using the subcutaneous implantation model confirm the mitigation of macrophage fusion and FBGC formation for BMG-55 implants. This finding is consistent with the reduction in CCL2 (MCP-1) secretion by IFN-γ/LPS-treated macrophages cultured on BMG-55 because this chemokine has been shown to be required for FBGC formation [36, 38, 55]. Currently, there is a paucity of information regarding the role of macrophage phenotype in macrophage fusion and FBGC formation. IL-4 is well known as a polarizing cytokine toward pro-healing phenotype. However, IL-4 also induces macrophage fusion and promotes inflammatory multi-nucleated giant cell formation. *In vivo* studies investigating the phenotypes in FBGCs demonstrate that they express both M1 (IL-1β, iNOS and TNF-α) and M2 (Arg-1, CD36 and IL-10) markers. These observations support the hypothesis that polarization of inflammatory and anti-inflammatory macrophages is a continuum rather than distinct phenotypes [4, 14, 36].

Following FBGC formation, fibroblasts are recruited, collagen fibers are deposited and ultimately a dense collagenous capsule is formed. The capsule isolates the biomaterial and hinders its integration with the surrounding tissue. It can also perturb the function of diffusion-dependent devices such as drug-delivery and sensor systems [56–59]. Positive effects of nanopatterning on macrophage polarization and subsequent cytokine release may explain the reduction of capsule thickness surrounding BMG-55 implants. It has been shown that Arg-1 expressing macrophages are actively involved in the regulation of wound healing and fibrosis. Arg-1 is an enzyme which metabolizes arginine and regulates the synthesis of amino acid proline (required for collagen synthesis); however, it can suppress fibrosis by inhibiting antigen-specific T cell responses and prevents excessive collagen deposition [60,

61]. Therefore, the higher expression ratio of Arg-1 to iNOS in macrophages present at sites adjacent to BMG-55 implants might be correlated to a reduction in capsule thickness.

In addition to the effect of nanopatterning on macrophage fusion, our *in vitro* findings demonstrate that phagocytosis of microspheres was enhanced in M1 cells on BMG-55. The opposite effects of BMG-55 on fusion versus phagocytosis is consistent with our previous observations of differential susceptibility of these processes to inhibitors of cytoskeletal remodeling [6, 37]. Specifically, we showed that unlike phagocytosis, IL-4 induced fusion was reduced in the presence of a Rac1 inhibitor [6, 37]. Interestingly, in the present study we observed an increase in phagocytosis during IFN-γ/LPS stimulation despite an overall reduction in M1 polarization. We believe that this could be due to nanopattern induced changes in cytoskeletal remodeling leading to the formation of filopodial projections. Such projections could enhance the rate of microsphere-cell interaction and overall phagocytosis. It should also be noted that we and others have shown that several macrophage functions including polarization can be modulated by actin reorganization and cell shape [62–64]. In addition, Liu *et al* found IFN-γ/LPS-activated macrophages on polydimethylsiloxane (PDMS) substrates exhibited a round and flattened morphology, while IL-4-activated cells increased their elongation [11]. Consistent with our findings, a previous study showed a positive correlation between TNF-α secretion and macrophage area on glass substrates, while on chitosan substrate, small and rounded cells were found to produce less TNF-α [65].

In the present study, angiogenesis was evaluated as another parameter of the FBR. Detection of vascular cells with CD31 antibody following 2-week implantation showed an increase in the number of endothelial cells and luminal structures around BMG-55 implants. After 4-week implantation, the blood vessel density reduced around implants. Different research studies have shown the temporal variation of vascularization in subcutaneous implantation of biomaterials are influenced by their chemical, biological and physical characteristics [66–68]. For example, polyvinyl alcohol (PVA) sponge also displayed a reduction in vascularization after 3-week compared to 2-week implantation in subcutaneous mouse model [68]. Association of macrophage polarization with vascularization is poorly understood. However, the ratio of M2 to M1 macrophages and the time of polarization are two parameters that have been observed to correlate with remodeling of injured tissues around implants. All macrophage phenotypes support vascular remodeling in distinct ways. For example, M1 macrophages predominantly secrete vascular endothelial growth factor (VEGF), which induces angiogenesis. Similarly, M2 macrophages increase the secretion of platelet-derived growth factor (PDGF) that induces vessel maturation [69–74]. Consistent with our results, several studies demonstrate increased vascularization associated with higher ratios of M2 to M1 macrophages [75, 76]. For example, Badylak *et al.,* demonstrated that increasing early the of M2 to M1 ratio following 2-week implantation was correlated with more constructive remodeling of biologically-derived implants [77].

In conclusion, our data suggest that nanopatterning of BMG substrates influences macrophage polarization *in vitro* and *in vivo. In vitro*, it leads to modulation of macrophage functions including altered activation and enhancement of phagocytosis. *In vivo*, it modulates the kinetics of the FBR including reduced FBGC formation and encapsulation

and increased neovascularization during the early phase of the FBR. Therefore, nanopatterning approaches could be used to develop advanced biomaterials capable of modulating the FBR.

5. Conclusion

This study suggests engineered surface nanotopography of BMGs as an effective tool to actively modulate the immune response. Results show that nanopatterned BMGs can regulate macrophage phenotypes and functions. BMG-55 decreased the secretion of pro-inflammatory cytokines in IFN-γ/LPS treated macrophages and enhanced the phagocytic abilities of these cells. During *in vivo* subcutaneous implantation more constructive tissue repair was observed around BMG-55 implants. It was accompanied with attenuated FBR at 2 weeks, higher vascularization, and increased M2 to M1 ratio. Hence, BMG-55 represents a promising candidate for designing more advanced implantable biomaterials. In addition, highly tunable nanorod arrays of BMGs provide a suitable platform to study the signaling pathways mediating macrophages polarization, phagocytosis, and fusion.

Supplementary Material

Refer to Web version on PubMed Central for supplementary material.

Acknowledgments

Funds from National Institutes of Health Grant (GM-072194) and CRISP (NSF MRSEC DMR 1119826) supported these studies. The fabrication of the nano-patterns was supported by the Department of Energy through the Office of Basic Energy Sciences (#DE SC0004889). Facilities used for this work were supported by Yale Institute for Nanoscience and Quantum Engineering and CRISP. We would also like to thank Laura Beth Moore and Renhao Wang for technical assistance. Authors declare no conflict of interest related to this study.

References

1. Kyriakides TR. Molecular events at tissue-biomaterial interface. In: Badylak SF, editorHost response to biomaterials. The impact of host response on biomaterial selection. Elsevier; New York: 2015. 81–116.
2. Anderson JM. Inflammation, wound healing, and the foreign body response. In: Ratner BD, Hoffman AS, Schoen FJ, Lemons JE, editorsBiomaterials science: An introduction to materials in medicine. Elsevier Inc; New York: 2013. 503–512.
3. Corradetti B. The Immune Response to Implanted Materials and Devices. Springer; New York: 2017.
4. Moore LB, Kyriakides TR. Molecular characterization of macrophage-biomaterial interactions. In: Lambris JD, Ekdahl KN, Ricklin D, Nilsson B, editorsImmune responses to biosurfaces. Springer; Cham: 2015. 109–122.
5. Chung L, Maestas JR, Housseau F, Elisseeff JH. Key players in the immune response to biomaterial scaffolds for regenerative medicine. Adv Drug Deliv Rev. 2017; 114:184–92. [PubMed: 28712923]
6. Jay SM, Skokos EA, Zeng J, Knox K, Kyriakides TR. Macrophage fusion leading to foreign body giant cell formation persists under phagocytic stimulation by microspheres in vitro and in vivo in mouse models. J Biomed Mater Res Part A. 2010; 93(1):189–99.
7. MacLauchlan S, Skokos EA, Meznarich N, Zhu DH, Raoof S, Shipley JM, Senior RM, Bornstein P, Kyriakides TR. Macrophage fusion, giant cell formation, and the foreign body response require matrix metalloproteinase 9. J Leukoc Biol. 2009; 85(4):617–26. [PubMed: 19141565]

8. Das A, Segar CE, Hughley BB, Bowers DT, Botchwey EA. The promotion of mandibular defect healing by the targeting of S1P receptors and the recruitment of alternatively activated macrophages. Biomaterials. 2013; 34(38):9853–62. [PubMed: 24064148]
9. Mantovani A, Sica A, Sozzani S, Allavena P, Vecchi A, Locati M. The chemokine system in diverse forms of macrophage activation and polarization. Trends Immunol. 2004; 25(12):677–86. [PubMed: 15530839]
10. Klopfleisch R. Macrophage reaction against biomaterials in the mouse model Phenotypes, functions and markers. Acta Biomaterialia. 2016; 43:3–13. [PubMed: 27395828]
11. McWhorter FY, Wang T, Nguyen P, Chung T, Liu WF. Modulation of macrophage phenotype by cell shape. PNAS. 2013; 110(43):17253–8. [PubMed: 24101477]
12. McWhorter FY, Davis CT, Liu WF. Physical and mechanical regulation of macrophage phenotype and function. Cell Mol Life Sci. 2015; 72(7):1303–16. [PubMed: 25504084]
13. Martinez FO, Gordon S. The M1 and M2 paradigm of macrophage activation: time for reassessment. F1000prime Rep. 2014; 6:6–13. [PubMed: 24592318]
14. Miron RJ, Bosshardt DD. OsteoMacs: Key players around bone biomaterials. Biomaterials. 2016; 82:1–9. [PubMed: 26735169]
15. Mosser DM, Edwards JP. Exploring the full spectrum of macrophage activation. Nat Rev Immunol. 2008; 8(12):958–69. [PubMed: 19029990]
16. Gordon S. The macrophage: past, present and future. Eur J Immunol. 2007; 37:S9–17. [PubMed: 17972350]
17. Rath M, Müller I, Kropf P, Closs EI, Munder M. Metabolism via arginase or nitric oxide synthase: two competing arginine pathways in macrophages. Front Immunol. 2014; 5:1–10. [PubMed: 24474949]
18. Garg K, Pullen NA, Oskeritzian CA, Ryan JJ, Bowlin GL. Macrophage functional polarization (M1/M2) in response to varying fiber and pore dimensions of electrospun scaffolds. Biomaterials. 2013; 34(18):4439–51. [PubMed: 23515178]
19. Ballotta V, Driessen-Mol A, Bouten CV, Baaijens FP. Strain-dependent modulation of macrophage polarization within scaffolds. Biomaterials. 2014; 35(18):4919–28. [PubMed: 24661551]
20. Hotchkiss KM, Reddy GB, Hyzy SL, Schwartz Z, Boyan BD, Olivares-Navarrete R. Titanium surface characteristics, including topography and wettability, alter macrophage activation. Acta Biomaterialia. 2016; 31:425–34. [PubMed: 26675126]
21. Brown BN, Ratner BD, Goodman SB, Amar S, Badylak SF. Macrophage polarization: an opportunity for improved outcomes in biomaterials and regenerative medicine. Biomaterials. 2012; 33(15):3792–802. [PubMed: 22386919]
22. Franz S, Rammelt S, Scharnweber D, Simon JC. Immune responses to implants a review of the implications for the design of immunomodulatory biomaterials. Biomaterials. 2011; 32(28):6692–709. [PubMed: 21715002]
23. Rostam HM, Singh S, Salazar F, Magennis P, Hook A, Singh T, Vrana NE, Alexander MR, Ghaemmaghami AM. The impact of surface chemistry modification on macrophage polarization. Immunobiology. 2016; 221(11):1237–46. [PubMed: 27349596]
24. Vishwakarma A, Bhise NS, Evangelista MB, Rouwkema J, Dokmeci MR, Ghaemmaghami AM, Vrana NE, Khademhosseini A. Engineering immunomodulatory biomaterials to tune the inflammatory response. Trends Biotechnol. 2016; 34(6):470–82. [PubMed: 27138899]
25. Lynn AD, Kyriakides TR, Bryant SJ. Characterization of the in vitro macrophage response and in vivo host response to poly (ethylene glycol)-based hydrogels. J Biomed Mater Res Part A. 2010; 93(3):941–53.
26. Blakney AK, Swartzlander MD, Bryant SJ. The effects of substrate stiffness on the in vitro activation of macrophages and in vivo host response to poly (ethylene glycol)-based hydrogels. J Biomed Mater Res Part A. 2012; 100(6):1375.
27. Tang D, Chen S, Hou D, Gao J, Jiang L, Shi J, Liang Q, Kong D, Wang S. Regulation of macrophage polarization and promotion of endothelialization by NO generating and PEG-YIGSR modified vascular graft. Mater Sci Eng C. 2017; 84:1–11.

28. Shojaee M, Wood KB, Moore LK, Bashur CA. Peritoneal pre-conditioning reduces macrophage marker expression in collagen-containing engineered vascular grafts. Acta Biomaterialia. 2017; 64:80–93. [PubMed: 28987784]
29. Lee CH, Kim YJ, Jang JH, Park JW. Modulating macrophage polarization with divalent cations in nanostructured titanium implant surfaces. Nanotechnology. 2016; 27(8):085101. [PubMed: 26807875]
30. Tan J, Zhao C, Wang Y, Li Y, Duan K, Wang J, Weng J, Feng B. Nano-topographic titanium modulates macrophage response in vitro and in an implant-associated rat infection model. RSC Adv. 2016; 6(113):111919–27.
31. Padmanabhan J, Augelli MJ, Cheung B, Kinser ER, Cleary B, Kumar P, Wang R, Sawyer AJ, Li R, Schwarz UD, Schroers J, Kyriakides TR. Regulation of cell-cell fusion by nanotopography. Sci Rep. 2016; 6
32. Padmanabhan J, Kinser ER, Stalter MA, Duncan-Lewis C, Balestrini JL, Sawyer AJ, Schroers J, Kyriakides TR. Engineering cellular response using nanopatterned bulk metallic glass. ACS Nano. 2014; 8(5):4366–4375. [PubMed: 24724817]
33. Kumar G, Tang HX, Schroers J. Nanomoulding with amorphous metals. Nature. 2009; 457:868–872. [PubMed: 19212407]
34. Schroers J. Processing of bulk metallic glass. Adv Mater. 2010; 22(14):1566–97. [PubMed: 20496386]
35. Schroers J, Kumar G, Hodges TM, Chan S, Kyriakides TR. Bulk metallic glasses for biomedical applications. JOM. 2009; 61(9):21–9.
36. Schroers J, Johnson WL. Ductile bulk metallic glass. Phys Rev Lett. 2004; 93(25):255506. [PubMed: 15697909]
37. Moore LB, Sawyer AJ, Charokopos A, Skokos EA, Kyriakides TR. Loss of monocyte chemoattractant protein-1 alters macrophage polarization and reduces NF kappa B activation in the foreign body response. Acta Biomaterialia. 2015; 11:37–47. [PubMed: 25242651]
38. Jay SM, Skokos E, Laiwalla F, Krady M, Kyriakides TR. Foreign body giant cell formation is preceded by lamellipodia formation and can be attenuated by inhibition of Rac1 activation. Am J Pathol. 2007; 7:632–640.
39. Anderson JA, Lamichhane S, Mani G. Macrophage responses to 316L stainless steel and cobalt chromium alloys with different surface topographies. J Biomed Mater Res A. 2016; 104(11):2658–72. [PubMed: 27324956]
40. Ma QL, Zhao LZ, Liu RR, Jin BQ, Song W, Wang Y, Zhang YS, Chen LH, Zhang YM. Improved implant osseointegration of a nanostructured titanium surface via mediation of macrophage polarization. Biomaterials. 2014; 35(37):9853–67. [PubMed: 25201737]
41. Li B, Cao H, Zhao Y, Cheng M, Qin H, Cheng T, Hu Y, Zhang X, Liu X. In vitro and in vivo responses of macrophages to magnesium-doped titanium. Sci Rep. 2017; 15:42707.
42. Lee RS, Hamlet SM, Ivanovski S. The influence of titanium surface characteristics on macrophage phenotype polarization during osseous healing in type I diabetic rats: a pilot study. Clin Oral Implants Res. 2017; 28(10):e159–e168. [PubMed: 27637574]
43. Hotchkiss KM, Reddy GB, Hyzy SL, Schwartz Z, Boyan BD, Olivares-Navarrete R. Titanium surface characteristics, including topography and wettability, alter macrophage activation. Acta Biomaterialia. 2016; 31:425–34. [PubMed: 26675126]
44. Lee S, Choi J, Shin S, Im YM, Song J, Kang SS, Nam TH, Webster TJ, Kim SH, Khang D. Analysis on migration and activation of live macrophages on transparent flat and nanostructured titanium. Acta Biomaterialia. 2011; 7(5):2337–44. [PubMed: 21232636]
45. Lu J, Webster TJ. Reduced immune cell responses on nano and submicron rough titanium. Acta Biomaterialia. 2015; 16:223–31. [PubMed: 25660564]
46. Takebe J, Itoh S, Okada J, Ishibashi K. Anodic oxidation and hydrothermal treatment of titanium results in a surface that causes increased attachment and altered cytoskeletal morphology of rat bone marrow stromal cells in vitro. J Biomed Mater Res. 2000; 51(3):398–407. [PubMed: 10880082]

47. Kulkarni M, Mazare A, Gongadze E, Perutkova Š, Kralj-Iglič V, Milošev I, Schmuki P, Iglič A, Mozetič M. Titanium nanostructures for biomedical applications. Nanotechnology. 2015; 26(6): 062002. [PubMed: 25611515]
48. Mendonça G, Mendonça DB, Aragao FJ, Cooper LF. Advancing dental implant surface technology from micron-to nanotopography. Biomaterials. 2008; 29(28):3822–35. [PubMed: 18617258]
49. Shayan M, Moradi M, Plakseychuk AY, Shankar R, Chun Y. Osteoblast cell response to oxide films formed on nanograin 316L stainless steel obtained by two-dimensional linear plane-strain machining. Mater Lett. 2016; 177:94–8.
50. Tan KS, Qian L, Rosado R, Flood PM, Cooper LF. The role of titanium surface topography on J774A. 1 macrophage inflammatory cytokines and nitric oxide production. Biomaterials. 2006; 27(30):5170–7. [PubMed: 16808973]
51. Verma SK, Leikina E, Melikov K, Chernomordik LV, Dodia R, Meunier B, Kay CW, Rich RR. Late stages of the synchronized macrophage fusion in osteoclast formation depend on dynamin. Biochem J. 2014; 464(3):293–300. [PubMed: 25336256]
52. Kim JH, Jin P, Duan R, Chen EH. Mechanisms of myoblast fusion during muscle development. Curr Opin Genetics Dev. 20151; 32:62–70.
53. Ogle BM, Cascalho M, Platt JL. Biological implications of cell fusion. Nat Rev Mol Cell Biol. 2005; 6(7):567–75. [PubMed: 15957005]
54. Terada N, Hamazaki T, Oka M, Hoki M, Mastalerz DM, Nakano Y, Meyer EM, Morel L, Petersen BE, Scott EW. Bone marrow cells adopt the phenotype of other cells by spontaneous cell fusion. Nature. 2002; 416(6880):542–5. [PubMed: 11932747]
55. Kyriakides TR, Foster MJ, Keeney GE, Tsai A, Giachelli CM, Clark-Lewis I, Rollins BJ, Bornstein P. The CC chemokine ligand, CCL2/MCP1, participates in macrophage fusion and foreign body giant cell formation. Am J Pathol. 2004; 165(6):2157–66. [PubMed: 15579457]
56. Frost M, Meyerhoff ME. In vivo chemical sensors: tackling biocompatibility. Anal Chem. 2006; 78(21):7370–7377. [PubMed: 17128516]
57. Santambrogio L. Biomaterials in regenerative medicine and the immune system. Springer; New York: 2015.
58. Nichols SP, Koh A, Storm WL, Shin JH, Schoenfisch MH. Biocompatible materials for continuous glucose monitoring devices. Chem Rev. 2013; 113(4):2528–49. [PubMed: 23387395]
59. Miron RJ, Bosshardt DD. Multinucleated Giant Cells: Good Guys or Bad Guys? Tissue Eng Part B Rev. 2018; 24(1):53–65. [PubMed: 28825357]
60. Pesce JT, Ramalingam TR, Mentink-Kane MM, Wilson MS, El Kasmi KC, Smith AM, Thompson RW, Cheever AW, Murray PJ, Wynn TA. Arginase-1-expressing macrophages suppress Th2 cytokine- driven inflammation and fibrosis. PLoS Pathog. 2009; 5(4):e1000371. [PubMed: 19360123]
61. Wynn TA, Vannella KM. Macrophages in tissue repair, regeneration, and fibrosis. Immunity. 2016; 44(3):450–62. [PubMed: 26982353]
62. Hoppe AD, Swanson JA. Cdc42, Rac1, and Rac2 display distinct patterns of activation during phagocytosis. Mol Biol Cell. 2004; 15(8):3509–19. [PubMed: 15169870]
63. Wheeler AP, Wells CM, Smith SD, Vega FM, Henderson RB, Tybulewicz VL, Ridley AJ. Rac1 and Rac2 regulate macrophage morphology but are not essential for migration. J Cell Sci. 2006; 119(13):2749–57. [PubMed: 16772332]
64. Kilian KA, Bugarija B, Lahn BT, Mrksich M. Geometric cues for directing the differentiation of mesenchymal stem cells. Proc Natl Acad Sci. 2010; 107(11):4872–7. [PubMed: 20194780]
65. Lee HS, Stachelek SJ, Tomczyk N, Finley MJ, Composto RJ, Eckmann DM. Correlating macrophage morphology and cytokine production resulting from biomaterial contact. J Biomed Mater Res Part A. 2013; 101(1):203–12.
66. Anderson JM. Biological responses to materials. Annu Rev Mater Sci. 2001; 31(1):81–110.
67. Alcaide M, Taylor A, Fjorback M, Zachar V, Pennisi CP. Boron-doped nanocrystalline diamond electrodes for neural interfaces: in vivo biocompatibility evaluation. Front Neurosci. 2016; 10
68. Kyriakides TR, Zhu YH, Yang Z, Huynh G, Bornstein P. Altered extracellular matrix remodeling and angiogenesis in sponge granulomas of thrombospondin 2-null mice. Am J Pathol. 2001; 159(4):1255–62. [PubMed: 11583953]

69. Simons M, Alitalo K, Annex BH, Augustin HG, Beam C, Berk BC, Byzova T, Carmeliet P, Chilian W, Cooke JP, Davis GE. State-of-the-art methods for evaluation of angiogenesis and tissue vascularization: a scientific statement from the American Heart Association. Circ Res. 2015; 116(11):e99–132. [PubMed: 25931450]

70. Spiller KL, Nassiri S, Witherel CE, Anfang RR, Ng J, Nakazawa KR, Yu T, Vunjak-Novakovic G. Sequential delivery of immunomodulatory cytokines to facilitate the M1-to-M2 transition of macrophages and enhance vascularization of bone scaffolds. Biomaterials. 2015; 37:37194–207.

71. Spiller KL, Anfang RR, Spiller KJ, Ng J, Nakazawa KR, Daulton JW, Vunjak-Novakovic G. The role of macrophage phenotype in vascularization of tissue engineering scaffolds. Biomaterials. 2014; 35(15):4477–88. [PubMed: 24589361]

72. Sunderkötter C, Steinbrink K, Goebeler M, Bhardwaj RA, Sorg C. Macrophages and angiogenesis. J Leukoc Biol. 1994; 55(3):410–22. [PubMed: 7509844]

73. Fishman JM, Lowdell MW, Urbani L, Ansari T, Burns AJ, Turmaine M, North J, Sibbons P, Seifalian AM, Wood KJ, Birchall MA. Immunomodulatory effect of a decellularized skeletal muscle scaffold in a discordant xenotransplantation model. Proc Natl Acad Sci. 2013; 110(35): 14360–5. [PubMed: 23940349]

74. Eaton KV, Yang HL, Giachelli CM, Scatena M. Engineering macrophages to control the inflammatory response and angiogenesis. Exp Cell Res. 2015; 339(2):300–9. [PubMed: 26610863]

75. Madden LR, Mortisen DJ, Sussman EM, Dupras SK, Fugate JA, Cuy JL, Hauch KD, Laflamme MA, Murry CE, Ratner BD. Proangiogenic scaffolds as functional templates for cardiac tissue engineering. Proc Natl Acad Sci. 2010; 107(34):15211–6. [PubMed: 20696917]

76. Jetten N, Verbruggen S, Gijbels MJ, Post MJ, De Winther MP, Donners MM. Anti-inflammatory M2, but not pro-inflammatory M1 macrophages promote angiogenesis in vivo. Angiogenesis. 2014; 17(1):109–18. [PubMed: 24013945]

77. Brown BN, Londono R, Tottey S, Zhang L, Kukla KA, Wolf MT, Daly KA, Reing JE, Badylak SF. Macrophage phenotype as a predictor of constructive remodeling following the implantation of biologically derived surgical mesh materials. Acta Biomaterialia. 2012; 8(3):978–87. [PubMed: 22166681]

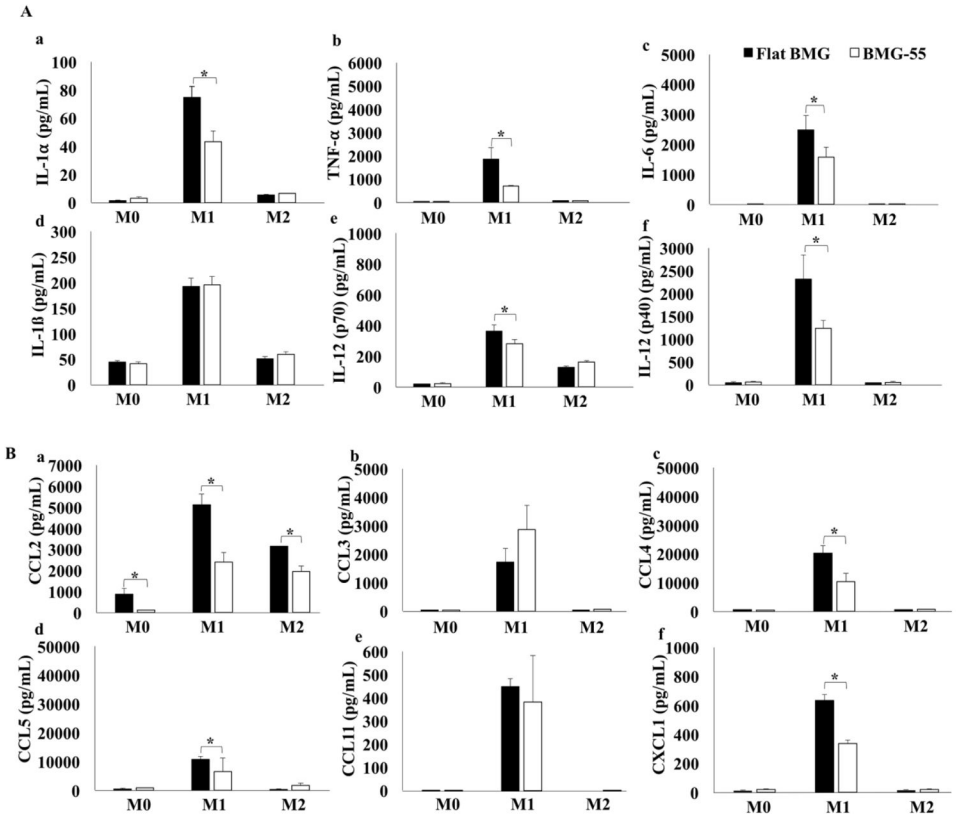

Fig. 1.

Concentration of pro-inflammatory cytokines and chemokines released by M0, M1 and M2 cells after 24hrs culture on BMG substrates. Levels were quantified with a 23-plex Luminex panel. (A) Levels of cytokines are shown including IL-1α (a), TNF-α (b), IL-6 (c), IL-1β (d), IL-12 (p70) (e), and IL-12 (p40) (f). (B) Levels of chemokines are shown including CCL2 (a), CCL3 (b), CCL4 (c), CCL5 (d), CCL11 (e), CXCL1 (f). Data represent mean + SD (*p ≤0.05) (n=3).

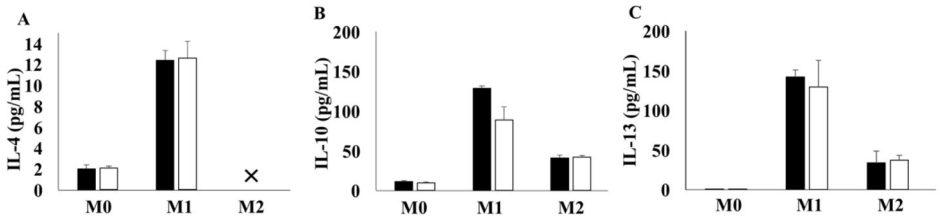

Fig. 2.

Concentration of anti-inflammatory cytokines released by M0, M1 and M2 cells after 24hrs culture on flat BMG or BMG-55 substrates. Cytokines levels were quantified with a 23-plex Luminex panel. Concentration of anti-inflammatory cytokines are shown including IL-4 (A), IL-10 (B) and IL-13 (C). The level of released IL-4 by M2 cells are out of measurement range (>) (✕) because of exogenously added IL-4. Data represent mean + SD (n=3).

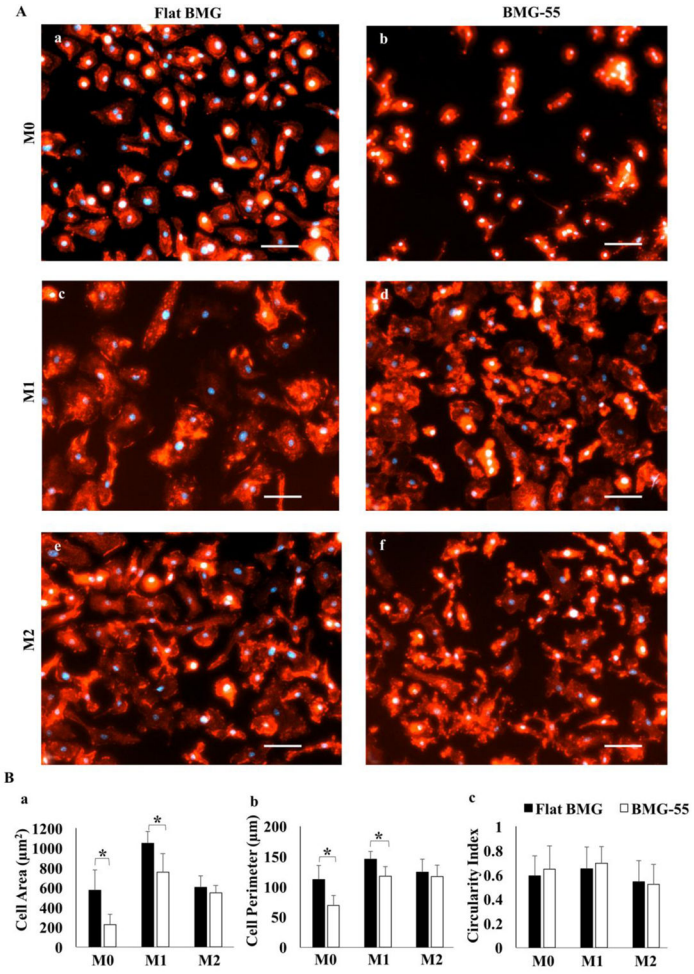

Fig. 3.

Nanopatterning influences cell morphology. Fluorescent images of M0, M1 and M2 cells stained with DAPI (blue) and rhodamine Phalloidin (red) on Flat BMG (A: a, c, e) or BMG-55 (A, b, d, f). Scale bar = 20μm. Original magnification, 200×. (B) Quantification of cell morphology including area (a), perimeter (b), and circularity (c). M0 and M1 cells were smaller on BMG-55. Data represent mean + SD (*$p \leq 0.05$), (n=5).

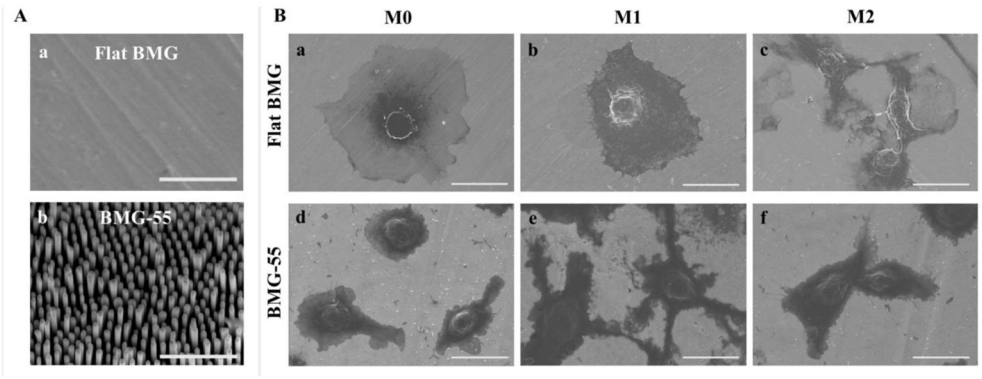

Fig. 4.

Representative SEM images of the surface of Flat BMG (A, a) and BMG-55 (A, b). Scale bar = 1μm. Representative SEM images of attached M0, M1 and M2 cells on Flat BMG (B, a–c) and BMG-55 (B, d–f) substrates. Scale bar = 20μm.

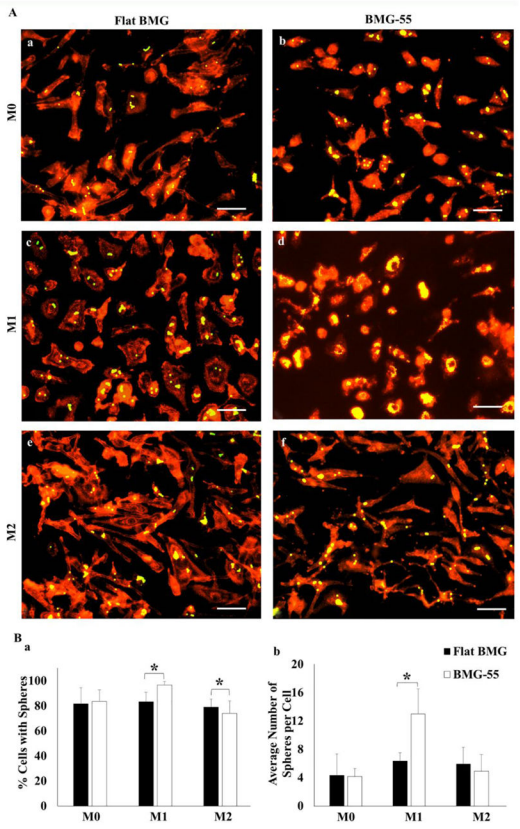

Fig. 5.

Nanopatterning influences uptake of microspheres. M0, M1 and M2 cells were exposed to Fluoresbrite® microspheres for 24hrs. Representative fluorescent images of uptake of microspheres (yellow) by cells stained with rhodamine Phalloidin (red) on Flat BMG (A: a, c, e) and BMG-55 (A: b, d, f). Scale bars = 20μm. Original magnification, 200×. Quantification of microsphere uptake measured as percentage of cells with spheres (B: a) and average number of spheres per cell (B: b). Data represent mean + SD (*$p \leq 0.05$), (n=5).

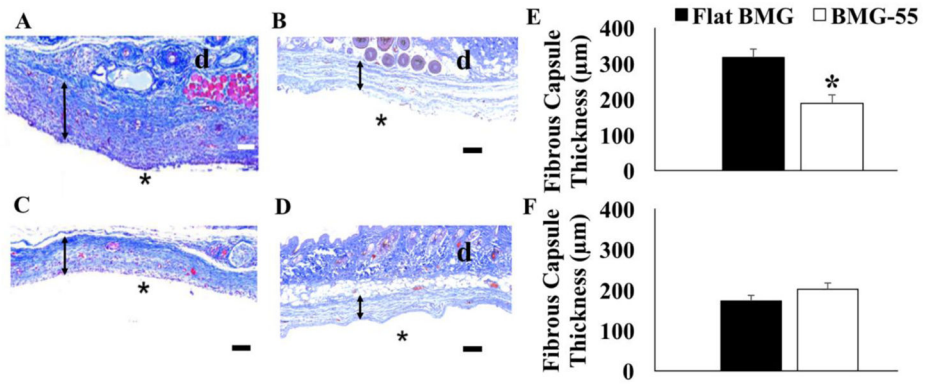

Fig. 6.

Assessment of fibrous capsules formation. Masson's trichrome staining highlights in dark blue the collagen fibers adjacent to the implants (*, denotes original implant location and d, denotes dermis). Flat BMG explanted after 2 (A), and 4 (B) weeks and BMG-55 explanted at 2 C) and 4 (D) weeks are shown. Fibrous capsule is indicated by bidirectional arrows. Scale bar = 100μm. Capsule thickness measurements at 2 and 4 weeks post-implantation are shown (E and F). Data represent mean values + SD (*p ≤0.05) (n=6).

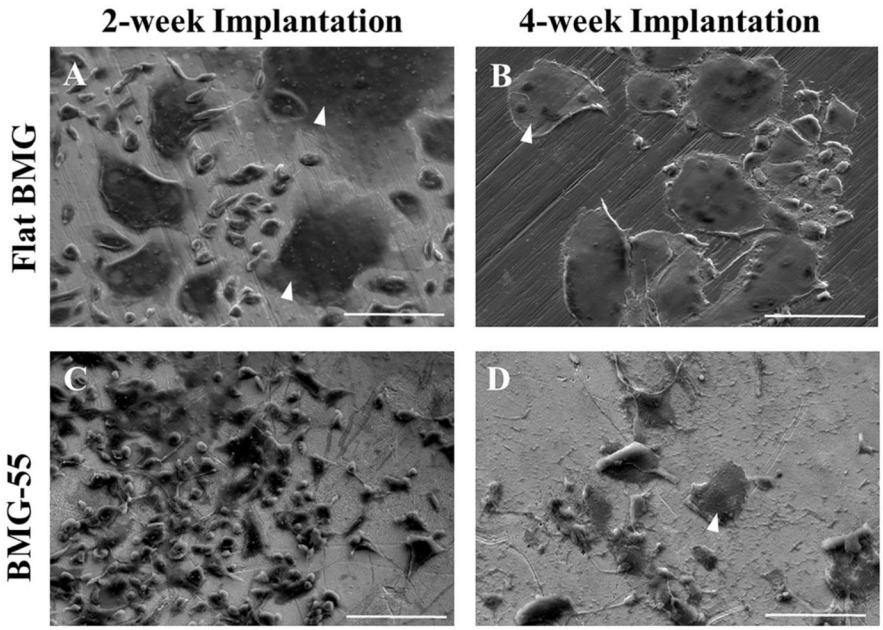

Fig. 7.

SEM analysis of SC implants. Representative images of individual cells and FBGC Fig. 7. SEM analysis of SC implants. Representative images of individual cells and FBGCweeks. FBGC are indicated by white arrowheads. Scale bar = 100μm.

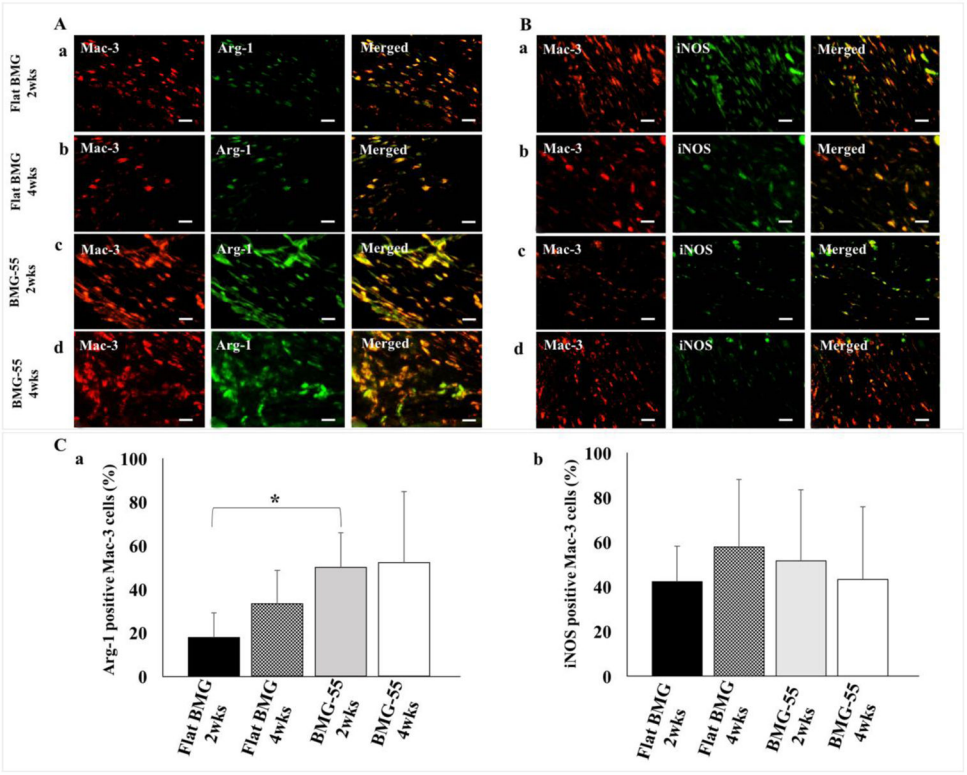

Fig. 8.

Macrophage polarization in the FBR. Representative images of sections of the FBR surrounding Flat BMG (A: a, b; B: a, b) and BMG-55 (A: c, d; B: c, d) disks that were mplanted SC in WT mice for 2 (A: a, c and B: a, c) or 4 (A: b, d and B: b, d) weeks are shown. (A) Sections were stained with antibodies against Mac-3 (Red) and Arg-1 (Green) or (B) Mac-3 (Red) and iNOS (Green). Scale bar = 20μm. Original magnification, 400×. Image analysis results are presented as the percentage of Arg-1 positive Mac-3 cells (C: a) or iNOS- positive Mac-3 cells (C: b) (mean values + SD). Percentage of Arg-1 positive cells was enriched on BMG-55 at 2 weeks. A total of 25 sections were analyzed; 5 per implant and 5 mice/group, (*p ≤0.05).

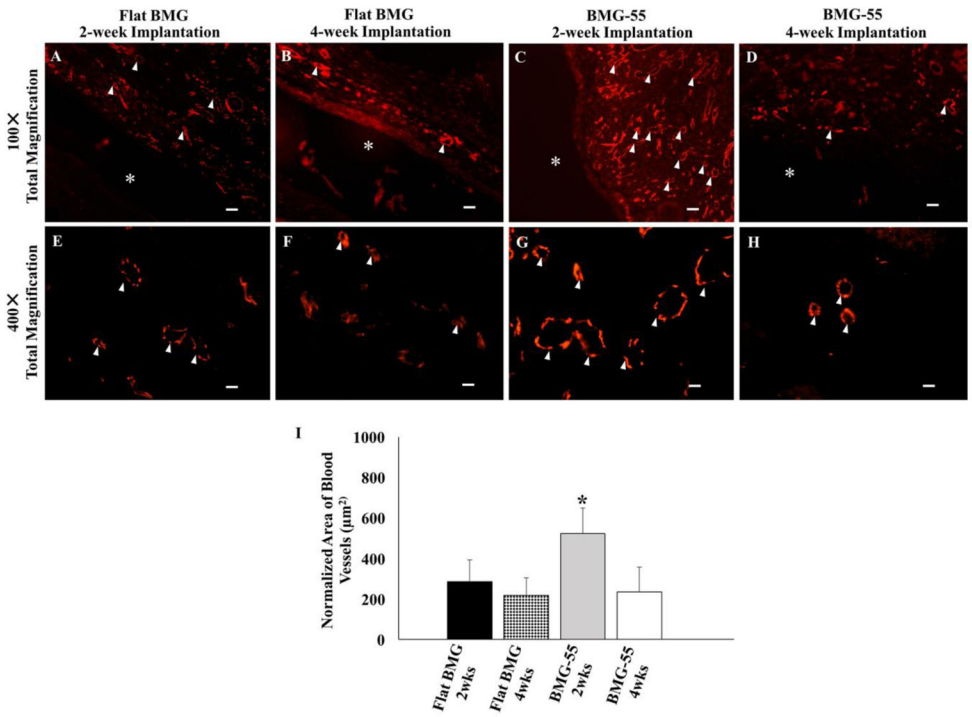

Fig. 9.

Nanopatterning influences neovascularization in the FBR. Representative low and high magnification images of sections of the FBR surrounding Flat BMG (A, B, E, F) and BMG-55 (C, D, G, H) disks that were implanted SC in WT mice for 2 (A, C, E, G) or 4 (B, D, F, H) weeks are shown. Sections were stained with CD-31 antibody to visualize vascular cells (Red). * denotes original implant location and white arrowheads denote blood vessels. Scale bar = 40μm (A–D) and 10μm (E–H). Original magnification, 100× (A–E) and 400× (E–H). (I) Image analysis of CD31-stained sections for normalized average area of blood vessels. BMG-55 elicited increased neovascularization at 2 weeks. n=5 mice/group; 5 sections per animal. Values represent mean + SD (*p ≤0.05).